Report No.
UCB/SEMM-2009/03

Structural Engineering
Mechanics and Materials

Stability Analysis of Bay Bridge Saddle Configuration

By

Sanjay Govindjee

October 2009

Department of Civil and Environmental Engineering
University of California, Berkeley

Stability Analysis of Bay Bridge Saddle Configuration

Sanjay Govindjee[1]
Structural Engineering, Mechanics, and Materials
Department of Civil Engineering
University of California, Berkeley
Berkeley, CA 94720

Abstract

In this brief note, we present the results of a full finite deformation analysis of a system similar to the Oakland-San Francisco Bay Bridge saddle repair system. The bars are assumed to be pre-stressed and pivot freely at their attachment points. The dimensions used are for illustration purposes but are in intended to be in the range of those associated with the real system. The saddle system is seen to be unstable as designed. If the attachment points are moved to lie between the main pins, then the system is seen to be stable (self-centering).

1 System

The Oakland-San Francisco Bay Bridge saddle repair system is shown in Fig. 1(left). This basic system was used to repair a cracked eye-bar on the bridge in early September 2009. In mid October 2009, the repair system failed in a dramatic fashion. It was re-installed with some modifications at the end of October 2009 but still retains the basic characteristics shown. It consists of two saddle pieces that cup to the upper and lower pins holding the eye-bars. The saddles are pulled together by four pre-stressed bars (two used in this simplified 2 dimensional analysis). In this analysis, the bars are assumed to be connected to the saddles by frictionless pivots. The primary degrees of freedom for the system are the rotations of the top and bottom saddles, θ_1 and θ_2, respectively. Each saddle can rotate independently of the other. With rotation, the attachment points for the bars move resulting in changes in strain in the bars. A proper analysis of this system requires the consideration of finite deformation kinematics since higher than second order kinematics are needed to make a definitive statement on the system's stability. Shown in Fig. 1(right) is an alternative configuration where the attachment points for the bars are inside the main-pins. This configuration is also analyzed.

2 System potential energy

The potential energy of the system consists of the stored elastic energy in the two bars.

$$\Pi(\theta_1,\theta_2) = \frac{1}{2}k\Delta_1^2(\theta_1,\theta_2) + \frac{1}{2}k\Delta_2^2(\theta_1,\theta_2)\,, \tag{1}$$

[1]e-mail: s_g@berkeley.edu

where k is the stiffness of the bars and Δ_i their length changes from their reference unstressed lengths L_i^o. The Δ_i depend on the pre-stressing and the rotations θ_1 and θ_2. In our evaluation we account for the bars going slack by setting the energy contribution to zero when the distance between the attachment points falls below the unstressed lengths. In our examples we have assumed a pre-stressing of 200 N/mm^2 (equivalent to a 1 milli $-$ strain pre-strain). The pre-strain displacement $\delta_i = L_i^o \epsilon_{pre}$ and thus

$$\Delta_i = \delta_i + \left\| [\boldsymbol{R}(\theta_1)\boldsymbol{x}_i^{\rm top} + \boldsymbol{x}^{\rm pp}] - \boldsymbol{R}(\theta_2)\boldsymbol{x}_i^{\rm bottom} \right\| - L_i^o \,, \tag{2}$$

where $\boldsymbol{x}_i^{\rm top}$ is the vector from the center of the upper main-pin to the top attachment point of the bar, $\boldsymbol{x}_i^{\rm bottom}$ is the vector from the center of the lower main-pin to the bottom attachment point of the bar, and $\boldsymbol{x}^{\rm pp}$ is the vector from the center of the lower main-pin to the center of the upper main-pin. The rotations

$$\boldsymbol{R}(\theta_i) = \begin{bmatrix} \cos(\theta_i) & -\sin(\theta_i) \\ \sin(\theta_i) & \cos(\theta_i) \end{bmatrix} \tag{3}$$

and account for full finite rotations which are important when considering the kinematics of the system when the saddles co-rotate. Stability of the system can be assessed by an examination of the structure of the potential energy with respect to kinematic variations; see e.g. classical texts such as [Timoshenko and Gere(1961), Fung(1965)].

2.1 Case 1: Installed configuration

Shown in Fig. 2 is the potential energy of the system with respect to the saddle rotations. When the saddles counter rotate the energy grows and the system is seen to be stable against this type of motion. A section cut of the energy surface for $\theta_1 = -\theta_2$ is shown in Fig. 3(top) to emphasize this point. Also shown in Fig. 3(middle,bottom) are the strains in the bars along this path. Depending upon the direction of rotation one bar unloads and the other loads. With excessive rotations individual bars can go slack. Shown in Fig. 4(top) is a section of the energy surface when the saddles co-rotate ($\theta_1 = \theta_2$). The system is seen to be *unstable* with respect to this motion. As shown in Fig. 4(middle,bottom), both bars release their pre-strain when the saddles co-rotate. Due to the concave potential energy profile, this unloading will occur spontaneously. The only restraint to this instability will come from friction between the main-pin and the saddle (or any hard rotation-stops that may exist in the system). It should also be noted that if either the top or bottom saddle is held in a stop and the other saddle is left free, then this configuration is stable; see Figs. 5 and 6.

2.2 Case 2: Alternative configuration

As an alternative to the as installed configuration, we also consider a configuration where the attachment points of the bars are placed between the main-pins as shown in Fig. 1(right). Figure 7 shows the potential energy of the system

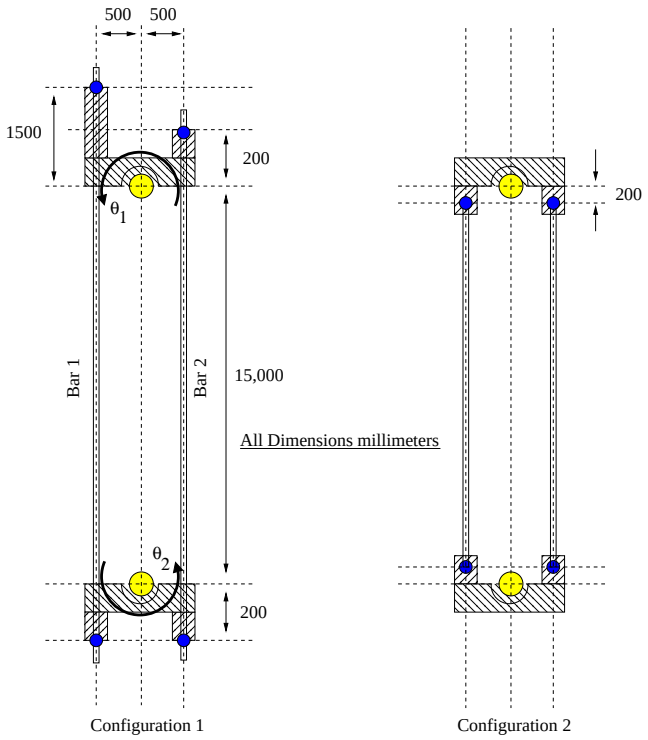

Figure 1: Configuration analyzed: (Left) Bar attachments above the main pins. (Right) Bar attachments between the main pins. Bars are assumed to be attached with pin joints (shown in blue). Drawing is **not to scale**. Assumed dimensions are given for illustrative purposes (actual values differ).

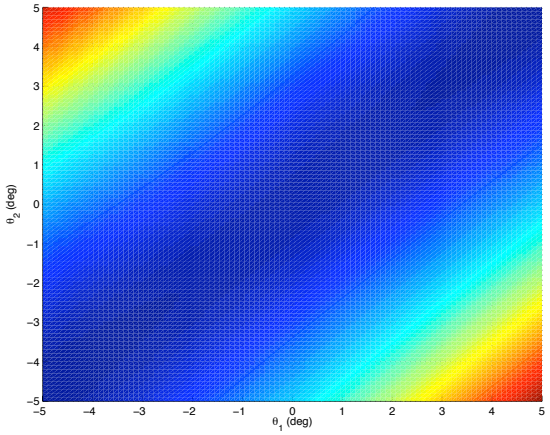

Figure 2: Potential energy in arbitrary units as a function of the saddle rotations for Case 1. Red values are higher than blue values. At the equilibrium point the energy possesses a saddle point structure.

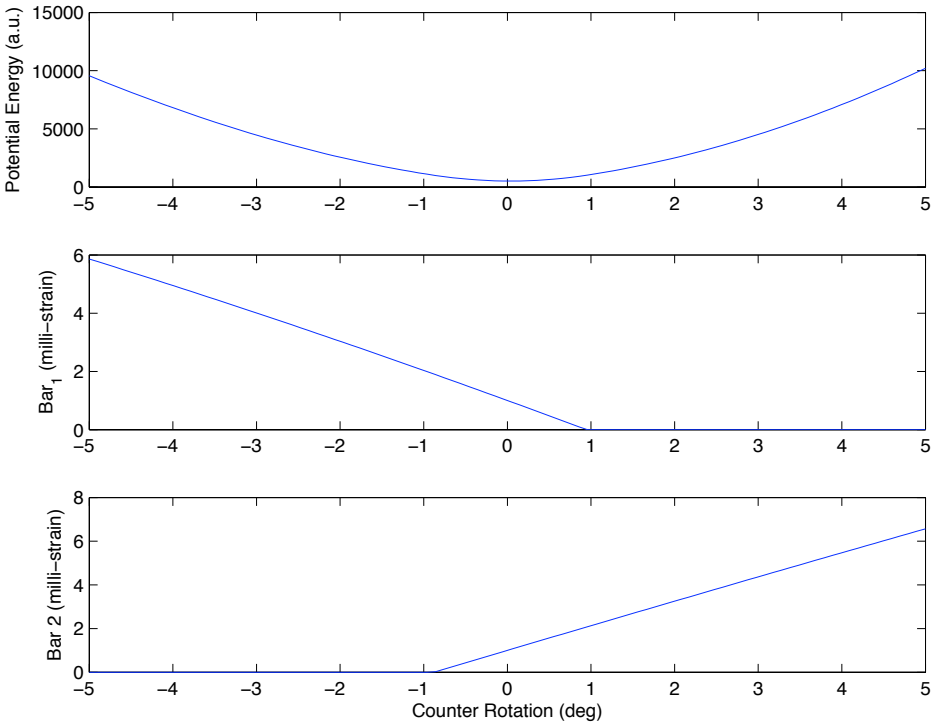

Figure 3: Case 1 System behavior for counter rotating saddles ($\theta_1 = -\theta_2$). (Top) Potential energy is seen to be stable. (Middle) Strain in bar 1. (Bottom) Strain in bar 2. Strains are zero when the bars go slack.

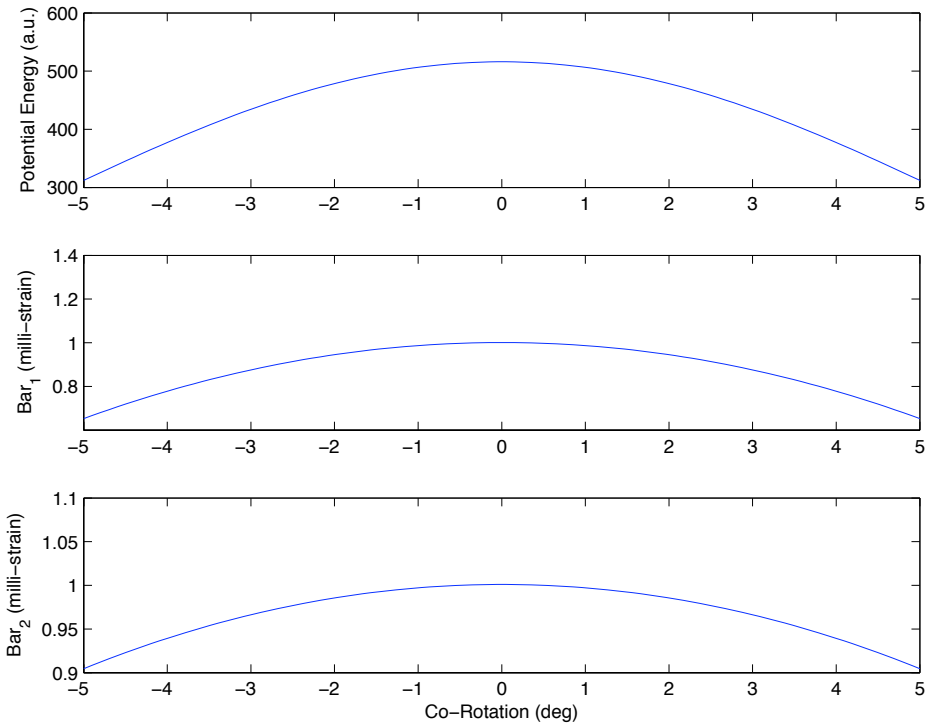

Figure 4: Case 1 System behavior for co-rotating saddles ($\theta_1 = \theta_2$). (Top) Potential energy is seen to be unstable. (Middle) Strain in bar 1. (Bottom) Strain in bar 2. Strains are zero when the bars go slack.

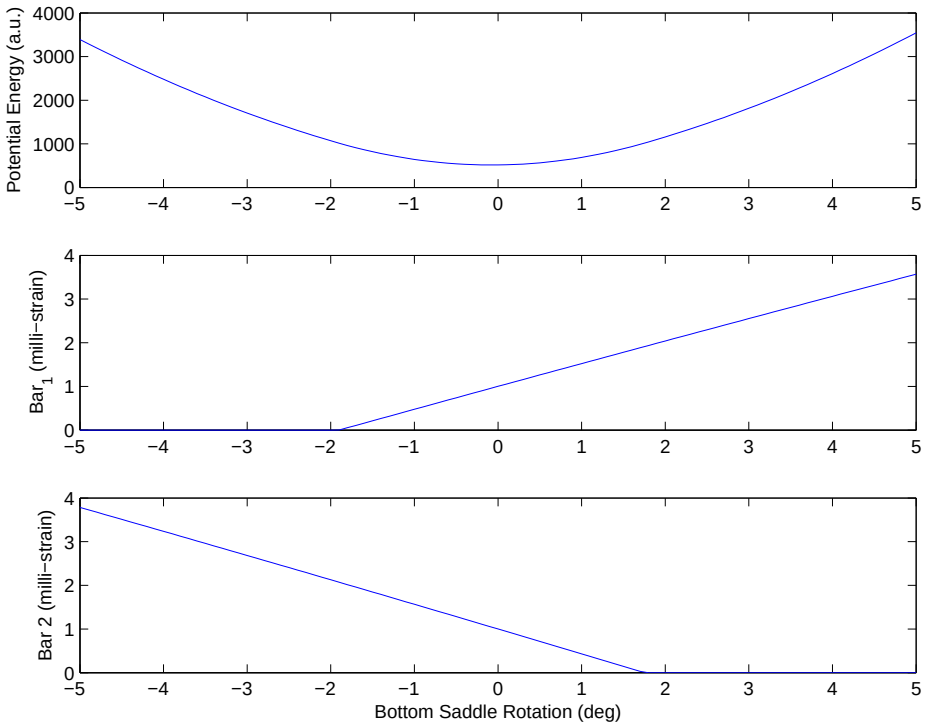

Figure 5: Case 1 System behavior with top saddle fixed ($\theta_1 = 0; \theta_2$ free). (Top) Potential energy is seen to be stable. (Middle) Strain in bar 1. (Bottom) Strain in bar 2. Strains are zero when the bars go slack.

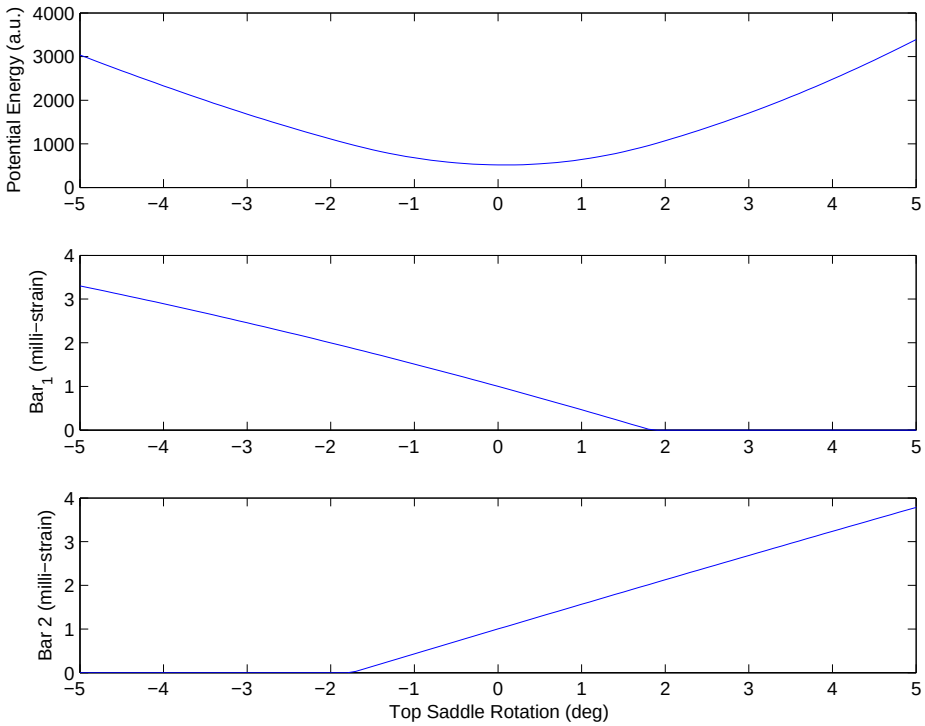

Figure 6: Case 1 System behavior with bottom saddle fixed (θ_1 free; $\theta_2 = 0$). (Top) Potential energy is seen to be stable. (Middle) Strain in bar 1. (Bottom) Strain in bar 2. Strains are zero when the bars go slack.

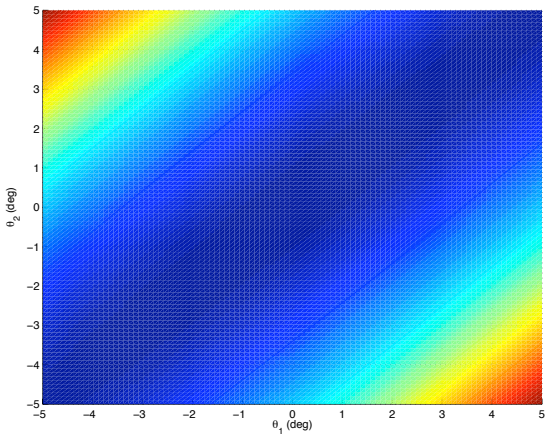

Figure 7: Potential energy in arbitrary units as a function of the saddle rotations for Case 2. Red values are higher than blue values. At the equilibrium point the energy possesses a (stable) bowl like structure.

with respect to the saddle rotations. When the saddles counter rotate the energy grows and the system is seen to be stable against this type of motion. A section cut of the energy surface for $\theta_1 = -\theta_2$ is shown in Fig. 8(top). This behavior is quite similar to Case 1. Also shown in Fig. 8(middle,bottom) are the strains in the bars along this path and they show similar behavior to Case 1. With excessive rotations individual bars can go slack as before. Shown in Fig. 9(top) is a section of the energy surface when the saddles co-rotate ($\theta_1 = \theta_2$). The system is seen now to be *stable* with respect to this motion in contradistinction to Case 1. As shown in Fig. 9(middle,bottom), both bars pick up strain when the saddles co-rotate and do not unload. Due to the convex potential energy profile, this mode of deformation will *not* occur spontaneously and thus the system is self-centering

3 Conclusion

A simple and straightforward analysis shows that the as designed repair system is inherently unstable and that a simple reconfiguration eliminates this problem. A broader question, which requires precise access to the system's geometry and properties, is whether or not this instability lead to the repair system's failure. Notwithstanding, it is clear that such instability is not helpful and can in the mind's eye easily lead to many deleterious effects, such as repeated large system motions, transverse loads on truss-members, etc.

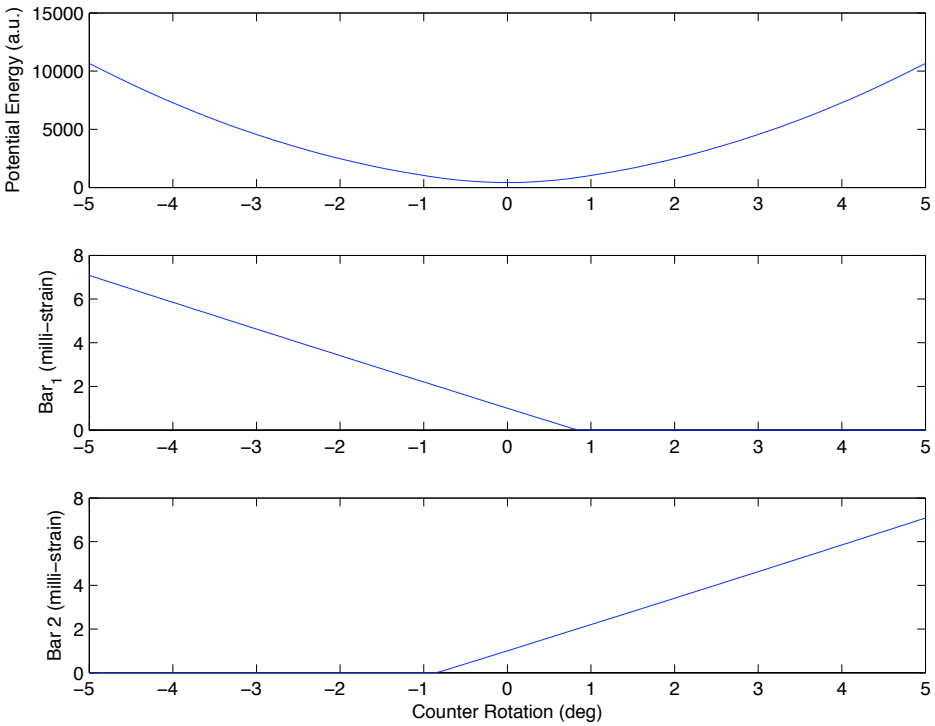

Figure 8: Case 2 System behavior for counter rotating saddles ($\theta_1 = -\theta_2$). (Top) Potential energy is seen to be stable. (Middle) Strain in bar 1. (Bottom) Strain in bar 2. Strains are zero when the bars go slack.

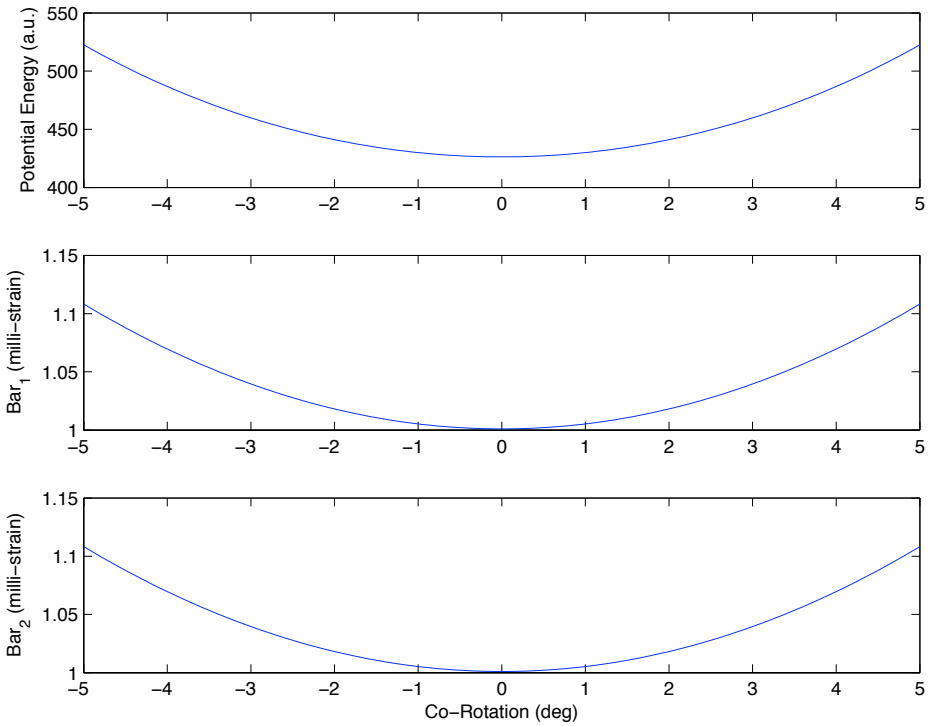

Figure 9: Case 2 System behavior for co-rotating saddles ($\theta_1 = \theta_2$). (Top) Potential energy is seen to be stable. (Middle) Strain in bar 1. (Bottom) Strain in bar 2. Strains are zero when the bars go slack.

References

[Fung(1965)] Fung, Y. C., 1965. Foundations of Solid Mechanics. Prentice-Hall.

[Timoshenko and Gere(1961)] Timoshenko, S., Gere, J., 1961. Theory of Elastic Stability. McGraw-Hill.